Journal of Alloys and Compounds 362 (2004) 3–11

Journal of ALLOYS AND COMPOUNDS

www.elsevier.com/locate/jallcom

# Correlation spectroscopy with coherent X-rays

Gerhard Grübel, Federico Zontone*

*European Synchrotron Radiation Facility, 6 rue Jules Horowitz BP 220, 38043 Grenoble Cedex 09, France*

Received 17 June 2002; accepted 16 September 2002

**Abstract**

X-ray photon correlation spectroscopy (XPCS) is a novel technique for the study of slow dynamics in disordered materials. It overcomes limitations of visible light scattering techniques such as multiple scattering or limitations in *Q*-range by using coherent X-rays from third generation synchrotron radiation sources. Applications to the static and dynamic behavior of complex fluids and to slow dynamics in hard condensed matter systems are reviewed.


*Keywords:* X-ray photon correlation spectroscopy (XPCS); Photon correlation spectroscopy; Speckle; Coherent X-rays; Colloidal suspensions; Capillary waves; Non-equilibrium dynamics; Magnetic disorder

## 1. Introduction

One of the outstanding properties of third generation synchrotron radiation sources is their capability of producing coherent X-ray beams several orders of magnitude more intense than previously available. The access to coherent X-rays opens up a variety of possibilities for new techniques such as X-ray photon correlation spectroscopy [1–5], static X-ray speckle analysis and metrology [6] and has major impact on imaging techniques such as topography [7], phase-contrast and holographic imaging [8,9]. Much of the excitement about scattering with coherent X-rays stems from the perspective to perform atomic resolution correlation spectroscopy and we will focus in this paper on the progress towards studying the complex dynamics of disordered systems on length- and time-scales inaccessible to other techniques.

If coherent light is scattered from a disordered system it gives rise to a random diffraction or 'speckle' pattern. Speckle patterns, long known from laser light scattering [10] and more recently also observed with coherent X-rays [11], are related to the exact spatial arrangement of the disorder. Such information is inaccessible with incoherent light because the diffraction pattern is, in this case, typically an ensemble average containing information on the average correlations in the sample. If the spatial arrangement of the disorder changes with time the corresponding speckle pattern will also change and the intensity fluctuations of a speckle can provide a measure of the underlying dynamics. X-ray photon correlation spectroscopy (XPCS) probes the dynamic properties of matter by analyzing the temporal correlations among photons scattered by the studied material. It typically measures the low frequency dynamics ($10^6$ Hz to $10^{-3}$ Hz) in a $Q$ range from typically $1 \times 10^{-3}$ Å$^{-1}$ up to several Å$^{-1}$. Fig. 1 shows the frequency–wavevector range accessible to this technique compared to other methods frequently used to study the dynamics in disordered systems.

XPCS is a young technique but has already shown the potential to impact several areas of statistical physics and provide access to a variety of important dynamic phenomena. Among them are the time-dependence of equilibrium critical fluctuations and the low frequency dynamics in disordered hard (e.g. non-equilibrium dynamics in phase separating alloys or glasses) and soft condensed matter materials, in particular complex fluids (e.g. hydrodynamic modes in concentrated colloidal suspensions, capillary mode dynamics in liquids and layer-fluctuations in membranes, equilibrium dynamics in polymer systems).

* Corresponding author. Tel.: +33-4-7688-2555; fax: +33-4-7688-2160.
*E-mail address:* zontone@esrf.fr (F. Zontone).

0925-8388/$ – see front matter © 2003 Elsevier B.V. All rights reserved.
doi:10.1016/S0925-8388(03)00555-3

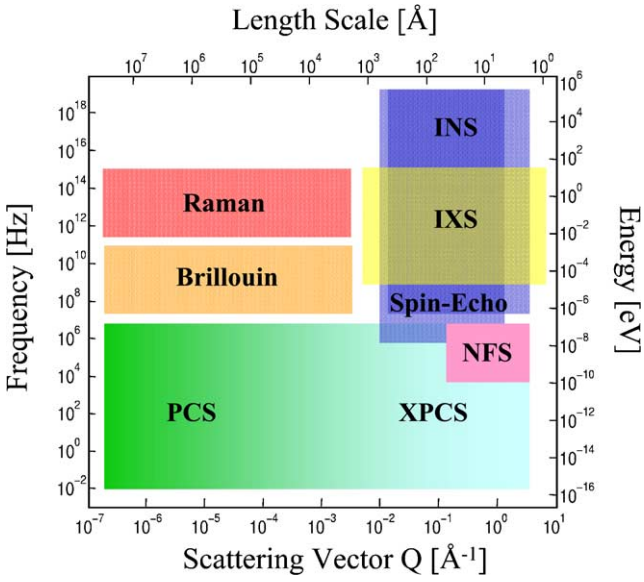


Fig. 1. Frequency–scattering vector space covered by X-ray photon correlation spectroscopy (XPCS) and complementary techniques: photon correlation spectroscopy with visible coherent light (PCS), Raman and Brillouin scattering, inelastic neutron (INS) and X-ray scattering (IXS), neutron spin-echo and nuclear forward scattering (NFS).

## 2. Scattering with coherent X-rays

Undulator insertion devices are periodic magnet structures installed in the straight sections of a synchrotron storage ring producing a discrete spectrum of intense synchrotron radiation. The fraction $F_c$ of the undulator flux that is transversely coherent is given by [12]

$$F_c = (\lambda/2)^2 B \tag{2.1}$$

where $B$ is the brilliance of the source, given in units of photons/s/mrad$^2$/mm$^2$/0.1% bandwidth. The transverse coherence length $\xi_t$ of the photon beam can be defined via the visibility of interference fringes. A visibility $V > 50\%$ for a uniform monochromatic disk source of size $s$ yields [13,14]

$$\xi_t \approx (1/2)(\lambda/\Delta\Theta) = (\lambda/2)(R/s). \tag{2.2}$$

Typical transverse coherence lengths at third generation sources are 10 μm (horizontally) and 100 μm (vertically) for $\lambda = 1$ Å and a distance $R \approx 45$ m from a source with angular source size $\Delta\Theta = s/R$. The temporal coherence of the beam can be described by the longitudinal coherence length $\xi_l$ which depends upon the monochromaticity of the beam and

$$\xi_l \approx \lambda(\lambda/\Delta\lambda). \tag{2.3}$$

Table 1 gives values for the relative bandwidth, longitudinal coherence length and the coherent flux for different optical configurations. There are several other methods to characterize the coherence properties of synchrotron X-ray beams [7,15–17]. The statistical analysis of static speckle patterns [7] allows to measure and optimize the coherence parameters in exactly the same experimental configuration that is used for a dynamic XPCS measurement.

Table 1
Bandpass $\Delta\lambda/\lambda$, longitudinal coherence length $\xi_l$ at 1 Å wavelength and coherent flux $F_c$ ($B = 10^{20}$ phonons/s/0.1% bandwidth/mm$^2$/mrad$^2$) for Si(220), Si(111) and a configuration using the intrinsic bandwidth $\Delta\lambda/\lambda = 1/nN$ of the third ($n = 3$) harmonic of an $N = 35$ period undulator

| | $\Delta\lambda/\lambda$ | $\xi_l$ (μm) ($\lambda = 1$ Å) | $F_c$ ($B = 10^{20}$) |
|---|---|---|---|
| Si(220) | $6 \times 10^{-5}$ | 1.7 | $1.5 \times 10^{10}$ |
| Si(111) | $14 \times 10^{-5}$ | 0.7 | $3.5 \times 10^{10}$ |
| U ($n = 1$, $N = 35$) | $1 \times 10^{-2}$ | 0.01 | $2.5 \times 10^{12}$ |

Scattering experiments with coherent X-rays require the sample to be illuminated coherently, implying that the maximum path length difference (PLD) for rays in the sample has to be equal or smaller than the longitudinal coherence length $\xi_l$ of the beam. In addition, the lateral size of the illuminated sample volume must be smaller than or comparable to the transverse coherence length $\xi_t$. The maximum path length difference is

$$\text{PLD} \approx 2\mu \sin^2\Theta \text{ or PLD} \approx 2W \sin^2\Theta + d \sin 2\Theta \tag{2.4}$$

in reflection or transmission geometry, respectively. Here $\mu$ is the absorption length, $W$ is the sample thickness, $d \leq \xi_T$ is the beam size and $\Theta$ is the scattering angle. Eq. (2.4) sets a limit for the maximum wavevector transfer $Q_{max} = (4\pi/\lambda)\sin\Theta_{max}$ that is compatible with coherent illumination. A schematic set-up of the ID10A branch of the TROIKA beamline [18] at ESRF for experiments with coherent X-rays is shown in Fig. 2. Similar beamline set-ups are described in Ref. [19]. A perfect crystal monochromator or a short mirror are located 44.2 m from source in horizontal reflection geometry. A second mirror mounted on a bender is installed in vertical reflection geometry 0.8 m downstream of the first mirror (monochromator) in order to reduce the harmonic content. Collimating pinholes of different diameter $d$ are installed downstream of the second mirror. The asymmetric source size (values given for a high-β section of the ESRF storage ring) of 928 μm (h) and 23 μm (v) causes different transverse coherence lengths in the horizontal ($\xi_t = 3$ μm) and vertical ($\xi_t = 98$ μm) directions ($\lambda = 1$ Å, $R = 45$ m). It is desirable to tune the transverse coherence lengths such that they are matched to the correlation lengths in the sample under investigation. This can be achieved by either collimating and/or focusing the beam. The integrated coherent flux achieved at ID10A at ESRF with a perfect crystal Si(111) monochromator ($\Delta\lambda/\lambda = 10^{-4}$) through a 12 μm pinhole is about $10^9$ photons/s at 100 mA storage ring current and $\lambda = 1$ Å. The sample is kept at a distance $R_c < d^2/\lambda$ in the near field region of the pinhole. The experimentally observed angular size of an individual speckle is approximately given by $D_s = [(\lambda/d)^2 + (\Delta\Theta)^2]^{1/2}$,

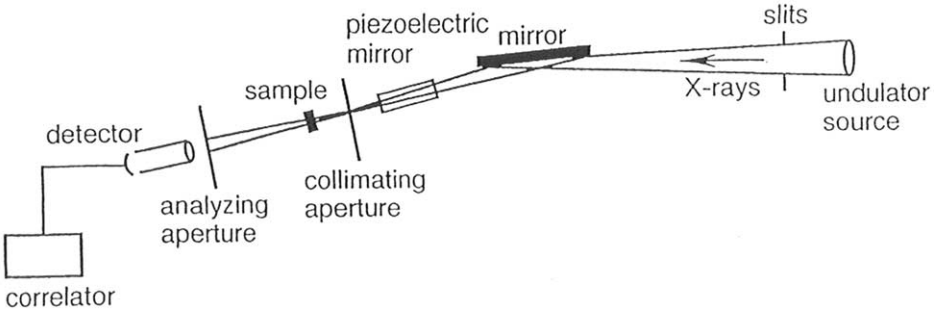


Fig. 2. Schematic set-up of the ID10A beamline at ESRF for coherent X-ray scattering. Typical distances are: source–deflecting mirror/monochromator, 44.2 m; deflecting mirror–focusing mirror, 0.8 m; focusing mirror–pinhole, 0.5 m; pinhole–sample, 0.1 m; sample–detector, 2 m.

where $\Delta\Theta$ is the effective angular source size. Speckle patterns can be recorded by either scanning a point detector combined with an analyser pinhole of diameter $< D_s$ in the scattered beam or by employing a one- or two-dimensional position-sensitive detector with the appropriate spatial resolution.

## 3. Disorder under coherent illumination

When coherent light is scattered from a disordered system it might give rise to a random diffraction or 'speckle' pattern. For illustration we consider a coherent beam of cross section $\xi_t^2$ and incident wave vector $\mathbf{k}$, scattered with outgoing wave vector $\mathbf{k}'$ from a disordered sample. The instantaneous intensity at a given point in the far field can be written as the square of a total field $E(\mathbf{Q}, t)$ and

$$I(\mathbf{Q}, t) = \left|E(\mathbf{Q}, t)\right|^2 = \left|\sum_n \exp[i\mathbf{Q}\cdot\mathbf{r}_n(t)] f_n(\mathbf{Q})\right|^2. \quad (3.1)$$

Here, $f_n(\mathbf{Q})$ is the scattering amplitude of the $n$-th scatterer located at position $\mathbf{r}_n(t)$, and $\mathbf{Q} = \mathbf{k}'-\mathbf{k}$ is the momentum transfer. The sum is taken over scatterers in the coherence volume, spanned by the transverse and longitudinal coherence lengths, and the beam is assumed to be fully coherent. For clarity we omit the Lorentz factor and the Thomson scattering length $r_o^2$ in Eq. (3.1). A measurement of the intensity will naturally be a time average $\langle I(\mathbf{Q}, t)\rangle_T$ taken over the acquisition time $T$, but does not involve any statistical ensemble average. If the system is non-ergodic, i.e. has static random disorder, $\langle I(\mathbf{Q}, t)\rangle_T$ will display, as a function of $\mathbf{Q}$, distinct and sharp (angular size $\lambda/\xi_t$) variations in intensity, known as 'speckle'. If, on the other hand, the system is ergodic, with fluctuation time scales very short to the counting time, the measured time average is equivalent to an ensemble average and $\langle I(\mathbf{Q}, t)\rangle_T$ can be replaced by the usual ensemble average, denoted by $\langle I(\mathbf{Q}, t)\rangle$. The observed scattering is then featureless apart from time averaged correlations in the sample similar to every scattering experiment with incoherent radiation. Fig. 3 (top) shows a static speckle pattern from a porous silica gel (aerogel) taken with a CCD detector and using an $E = 8.2$ keV coherent X-ray beam [7]. The 'random' nature of the scattering is illustrated by the solid line in Fig. 3 (bottom) showing a horizontal cut through the pattern with intensity variations significantly beyond counting statistics. The open symbols indicate the ensemble averaged scattering $\langle I(\mathbf{Q}, t)\rangle$, calculated from the speckle pattern by radial averaging.

Static X-ray speckle has been observed in a variety of different systems ranging from porous materials [17,20], modulated bulk and surface structures [21,22], surfaces [23] to (microscopic) domain disorder [2,11,24]. Methods to reconstruct the spatial arrangement of scatterers from a static speckle pattern [25–28] have become available recently and interferometric applications [29] are under development. A static speckle pattern contains however also information on the radiation that produced it, including the degree of coherency and the size of the illuminated volume. This in-

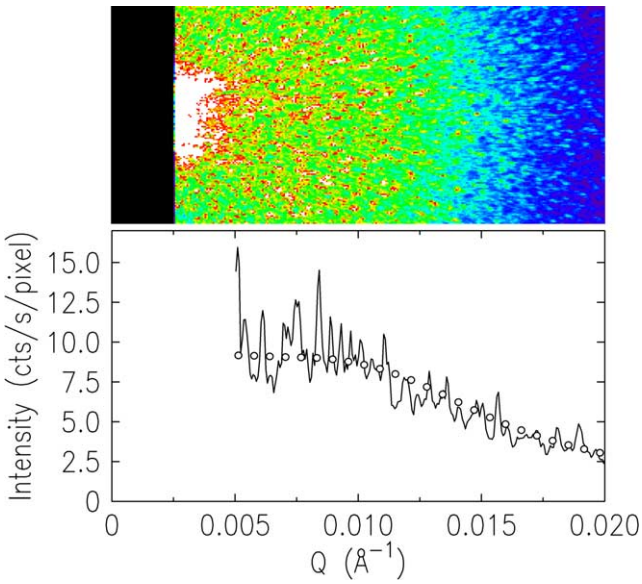


Fig. 3. Speckle pattern from an aerogel recorded with a 22 μm pixel size CCD detector using 8.2 keV coherent X-rays (top). Circular averaged scattering from the sample, normalized to give detected photons per second. The line is the intensity in one pixel row in the horizontal direction, showing the speckle structure (bottom) [17].

formation can be retrieved by a statistical analysis of static speckle patterns [17,20,30]. The effects of partial coherence of the X-ray beam have been analyzed in Ref. [31].

## 4. X-ray photon correlation spectroscopy (XPCS)

If the spatial arrangement of the scatterers changes with time the corresponding speckle pattern will also change and a measurement of the intensity fluctuations of the speckles can reveal the dynamics of the system. The measurement of temporal intensity correlations by X-ray photon correlation spectroscopy (XPCS) is identical to a photon correlation spectroscopy (PCS) experiment with visible coherent light, which is well documented in the literature [10]. Temporal correlations can be quantified with the help of the normalized intensity correlation function $g(\mathbf{Q}, t)$. If the system is ergodic the (time averaged) intensity correlation function can be written in terms of the (ensemble averaged) time correlation functions of the scattered field:

$$\begin{aligned} g(\mathbf{Q}, t) &= \langle I(\mathbf{Q}, 0) I(\mathbf{Q}, t)\rangle / \langle I(\mathbf{Q})\rangle^2 \\ &= 1 + \beta(\mathbf{Q}) \langle E(\mathbf{Q}, 0) E(\mathbf{Q}, t)\rangle^2 / \langle I(\mathbf{Q})\rangle^2 \end{aligned} \quad (4.1)$$

where $\beta(\mathbf{Q})$ is the contrast of the set-up. The time correlation function $g(\mathbf{Q}, t)$ is frequently expressed in terms of the normalized intermediate scattering function $f(\mathbf{Q}, t)$ with

$$g(\mathbf{Q}, t) = 1 + \beta(\mathbf{Q})[f(\mathbf{Q}, t)]^2 \quad (4.2)$$

where

$$f(\mathbf{Q}, t) = F(\mathbf{Q}, t)/F(\mathbf{Q}, 0) \quad (4.3)$$

and

$$F(\mathbf{Q}, t) = [1/Nf^2(\mathbf{Q})] \sum_n \sum_m \langle f_n(\mathbf{Q}) f_m(\mathbf{Q}) \times \exp\{i\mathbf{Q}[\mathbf{r}_n(0) - \mathbf{r}_m(t)]\}\rangle. \quad (4.4)$$

Here, $N$ is the number of scatterers, the brackets denote an ensemble average and $F(\mathbf{Q}, 0)$ can be identified with the static structure factor.

For illustration we consider in the following the simple example of monodisperse, spherical particles undergoing Brownian motion [10,32]. In the absence of interactions between the particles their positions are uncorrelated and cross ($n \neq m$) terms in (4.4) average to zero and $F(\mathbf{Q}, 0) = 1$. The mean square value of the displacement for a free Brownian particle is $\langle[\mathbf{r}(0) - \mathbf{r}(t)]^2\rangle = 6D_o t$, where $D_o$ is the free particle diffusion coefficient of a particle with radius $R$ and

$$D_o = k_B T/6\pi\eta R, \quad (4.5)$$

where $\eta$ is the shear viscosity of the surrounding medium. Thus (4.3) reduces to

$$f(\mathbf{Q}, t) = \exp(-D_o Q^2 t). \quad (4.6)$$

In the presence of particle interactions Eq. (4.6) is no longer valid and one frequently considers a time- and wavevector-dependent diffusion coefficient $D(Q, t)$ [33]. A useful quantity is the initial ($t \to 0$) slope $\Gamma(Q)$, or the first cumulant of the measured intermediate scattering function $f^M(Q, t)$, and it can be shown that

$$\Gamma(Q) = \lim_{t\to 0} \mathrm{d}/\mathrm{d}t[\ln f^M(Q, t)] = -D(Q)Q^2 \quad (4.7)$$

and

$$f(\mathbf{Q}, t) = \exp(-D(Q)Q^2 t). \quad (4.8)$$

Correlation functions can be measured by coupling a point detector to a digital autocorrelator giving fast access to the correlation function over a wide range of correlation times ($10^{-6}$ to $10^3$ s) at a single $Q$ value. Fig. 4 shows a typical intermediate scattering function (normalized to the contrast) taken on a concentrated suspension of colloidal PMMA particles. The measured data have been fitted with the cumulant expansion [10] using up to fourth order terms (solid black line). The behavior at very short times is described by the first cumulant $\Gamma(Q)$ (solid red line).

Two-dimensional position-sensitive detectors with appropriate spatial resolution (e.g. direct illuminated CCD cameras with 20 μm pixel size and about 40% quantum efficiency) can allow the collection of a complete speckle pattern covering the full range of $Q$ values. Correlation functions are then to be calculated for each pixel with subsequent ensemble averaging over equivalent $Q$ values [34,35]. CCD detectors are subject to limitations in read-out speed for a full 2-D pixel array and have been used up to now mostly for the study of very slow dynamics.

## 5. XPCS in soft condensed matter systems

### 5.1. Static and dynamic properties of colloidal suspensions

Colloidal suspensions [32] consist of colloidal particles (clusters of atoms or molecules) with typical diameters be-

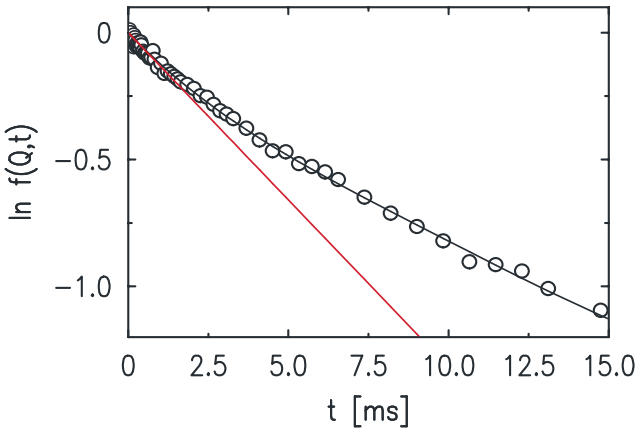


Fig. 4. Measured intermediate scattering function $f^M(Q, t)$ for a concentrated suspension of colloidal PMMA particles in *cis*-decalin. The solid black line shows a cumulant fit to the data using terms up to the fourth order. The red line shows the contribution of the first cumulant $\Gamma(Q)$.

tween 50 and 5000 Å that are suspended in a solvent (e.g. a molecular fluid). Agglomeration of the particles due to van der Waals attraction is prevented by introducing a repulsive (steric or coulombic) interaction between the particles. The interparticle interactions are then described by either a short-range pair potential (hard-spheres) or by a long-range Yukawa type potential (soft-spheres), respectively. The time-averaged structure of a colloidal suspension can be described by the static structure factor

$$S(Q) = 1 + 4\pi n \int [g(r) - 1](\sin(Qr)/Qr)r^2 \mathrm{d}r \qquad (5.1)$$

with $g(r) = \exp[-V(r)/kT]$ being the radial distribution function related to the potential $V(r)$ between two spheres separated by a distance $r$, and $n$ is the particle number density. In the dilute case ($n \ll 1$) and the absence of interparticle correlations, $S(Q) = 1$ and the colloidal particles migrate driven by the thermal fluctuations of the solvent, with the (free particle) diffusion coefficient $D_o$.

At larger concentrations direct interparticle interactions as well as indirect, hydrodynamic interactions, mediated by the solvent become important. Based on the Smoluchowski (many-particle diffusion) equation it has been shown that the short-time ($t < R^2/D_o$) behaviour of the intermediate scattering function can be described by an effective diffusion coefficient

$$D(Q) = D_o H(Q)/S(Q), \qquad (5.2)$$

where $H(Q)$ is the hydrodynamic function. The determination of $D(Q)$ and $S(Q)$ by PCS with visible light is a formidable task because of multiple scattering effects in dense, concentrated suspensions and due to the limited wavevector range. A consistent picture has nevertheless emerged for hard-sphere fluids on the basis of PCS work and analytical expressions for the structure factor (within the Percus–Yevick approximation [36]) and the hydrodynamic functions [37]. The situation for charge stabilized colloidal systems is considerably more complicated [38]. XPCS can offer two unique advantages compared to visible light scattering techniques: the short X-ray wavelength allows to access larger momentum transfers $Q$ and the technique is not subject to multiple scattering effects since the refractive index of X-rays is always very close to one. This allows to study turbid and optically opaque samples on all relevant lengthscales.

### 5.2. XPCS and SAXS measurements in colloidal suspensions

The static and dynamic behavior of colloidal suspensions can be fully determined by a combination of small angle X-ray scattering (SAXS) and XPCS. The cross section for the scattering of X-rays from a suspension of monodisperse colloidal particles can be written as

$$(\mathrm{d}\sigma/\mathrm{d}\Omega)/V = r_o^2 n(\rho_c - \rho_s)^2 v^2 |P(Q)|S(Q) \qquad (5.3)$$

where $r_o$ is the Thomson radius, $n = N/V$ is the number density of particles, $v$ is the particle volume and $\rho_c$, $\rho_s$ are the electronic densities of the colloid and the solvent, respectively. $P(Q)$ is the single particle form factor for a homogenous sphere with radius $R$ defined as

$$P(Q) = [f(Q)/f(0)]^2 = [3/(QR)^3]^2[\sin(QR) - QR\cos(QR)]^2 \qquad (5.4)$$

and $S(Q)$ is the static structure factor, describing interparticle correlations.

The first X-ray time correlation functions from a suspension of colloidal Au particles were reported by Dierker et al. [3] followed by the observation of translational diffusion of colloidal Pd agglomerates in glycerol [4]. Static and dynamic data taken on a model system, a dilute suspension of colloidal silica in a 1:1 mixture of water/glycerol (1% volume concentration), are shown in Fig. 5 [39]. The top panel shows the scattering intensity as a function of the momentum transfer showing pronounced oscillations that are perfectly described by the particle form factor (5.4), convoluted with a Shultz size distribution function yielding $R = 2427$ Å and $\Delta R/R = 4.5\%$. X-ray time correlation functions were taken over the whole $Q$ range and fit to a

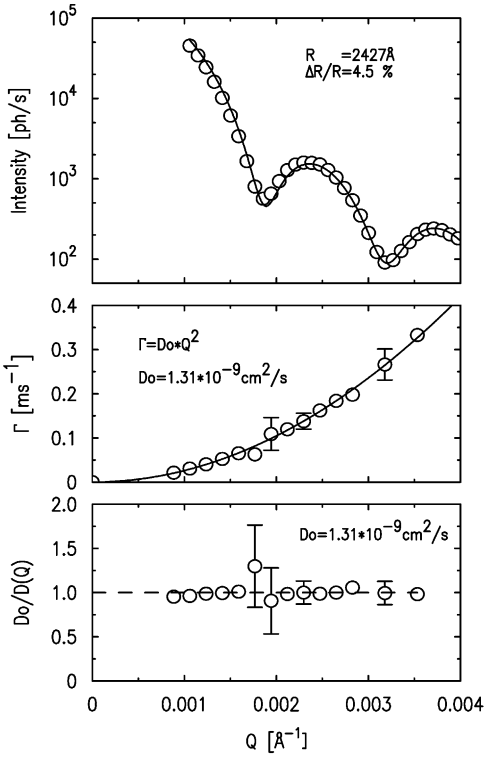


Fig. 5. X-ray small angle scattering intensity as a function of the momentum transfer $Q$ for a 1 vol.% suspension of colloidal silica ($R = 2427$ Å) in a glycerol/water mixture at 293 K (top). $Q$ dependence of the correlation rate $\Gamma$ as determined from intensity correlation functions taken at various $Q$ values (middle). The solid line is the result of a fit to the data with $D_o$ as a fit parameter. Normalized, inverse diffusion coefficient $D_o/D(Q)$ as a function of $Q$ (bottom) [39].

single exponential decay of Eq. (4.6) and the extracted correlation rate $\Gamma$ is plotted in the middle panel. The solid line reveals the characteristic $Q^2$ dependence of a simple translational diffusion process with $D_o = 1.31 \times 10^{-9}$ cm$^2$/s. This is also illustrated in the bottom panel where $D_o/D(Q)$ is plotted.

Both the static and dynamic behavior changes dramatically when the colloidal particles interact. This is illustrated for a hard-sphere model system, colloidal poly-methyl-methacrylate (PMMA) particles ($R = 1112$ Å) suspended with a volume fraction $\Phi = 0.37$ in *cis*-decalin [40]. Fig. 6a shows the scattering intensity as a function of the momentum transfer $Q$. The data at low $Q$ can no longer

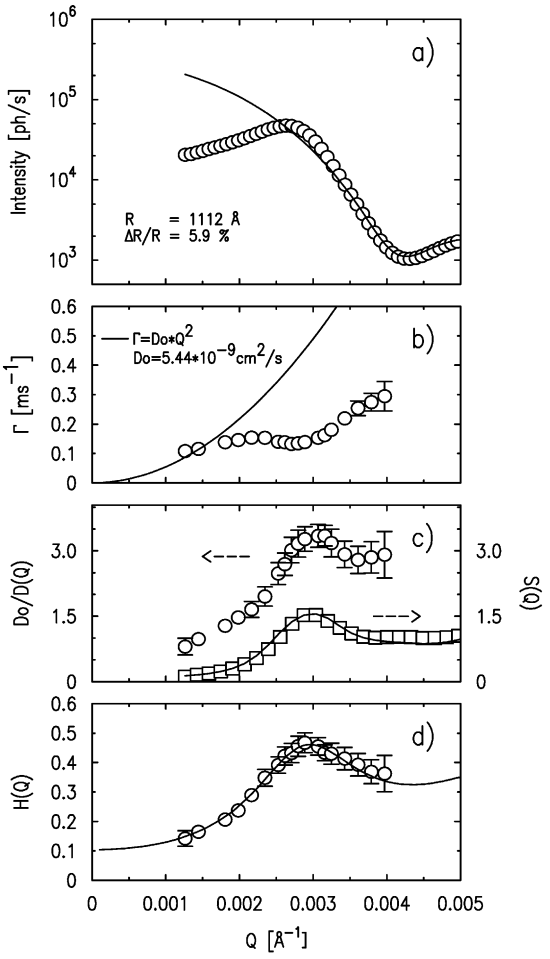


Fig. 6. X-ray small angle scattering intensity as a function of the momentum transfer $Q$ for a 37.3 vol.% suspension of colloidal PMMA particles ($R = 1112$ Å) in *cis*-decalin at 293 K. The solid line describes the particle form factor (Eq. (5.4)) and deviations are due to interparticle correlations $S(Q)$. (b) $Q$ dependence of the correlation rate $\Gamma$. The solid line is the result of a fit to the dilute data (not shown) with $D_o$ as a fit parameter. (c) Normalized, inverse diffusion coefficient $D_o/D(Q)$ as a function of $Q$ [40], compared to the static (time-averaged) structure factor $S(Q)$. The solid line is a calculated Percus–Yevick hard-sphere structure factor for $\Phi = 37.3\%$. (d) Hydrodynamic function $H(Q) = S(Q)/(D_o/D(Q))$. The solid line is the result of a model calculation (see text).

be described by the particle form factor (solid line) but contains the effects of the direct inter-particle interactions. These can be quantified by the static structure factor $S(Q)$ derived by dividing the measured data $I(Q)$ by the form factor $P(Q)$ and shown in Fig. 6c by the open squares. The hard-sphere character of the interactions is confirmed by the fact that $S(Q)$ is well described by a Percus–Yevick [36] structure factor shown by the solid line describing the $S(Q)$ data. Important differences to the dilute case are also observed in the dynamic behavior. Fig. 6b shows the correlation rates in the concentrated sample (open circles) compared to the diffusive behavior in the dilute case (solid line). The normalized inverse diffuse coefficient $D_o/D(Q)$ is shown in Fig. 6c. There is a pronounced maximum at $Q \approx 0.003$ Å$^{-1}$ that coincides with the peak in the static structure factor showing that the most likely density fluctuations decay the slowest. It is furthermore evident that $D_o/D(Q)$ is similar but not equal to $S(Q)$. This shows that indirect, hydrodynamic interactions are important for the system and the corresponding hydrodynamic function $H(Q)$ was derived using Eq. (5.2) with the result shown in Fig. 6d. The hydrodynamics of the hard-sphere system is usually modeled in terms of the $\delta$–$\gamma$ expansion developed by Beenakker and Mazur [37]. The hydrodynamic function can be expressed in terms of the static structure factor $S(Q)$ where $\Phi$ is the volume fraction and $S_{\gamma 0}$ a function defined in [37]:

$$
\begin{aligned}
H(Q) &= \frac{D_S(\Phi)}{D_0} \\
&\quad + \frac{3}{2\pi}\int_0^\infty \mathrm{d}(RQ')\,\frac{\dfrac{\sin(RQ')}{RQ'}}{1+\Phi S_{\gamma_0}(RQ')} \\
&\quad \times \int_{-1}^{1}\mathrm{d}x(1-x^2)\left[S(|Q-Q'|)-1\right], \\
\frac{D_S(\Phi)}{D_0} &= \frac{2}{\pi}\int_0^\infty \mathrm{d}x\left(\frac{\sin(x)}{x}\right)^2\left[1+\Phi S_{\gamma_0}(x)\right]^{-1}, \\
x &= \cos(Q-Q').
\end{aligned}
\tag{5.5}
$$

The solid line in Fig. 6d is the calculated hydrodynamic function by using the measured $S(Q)$ as the input. The agreement with the experimental data, which have been derived free from any modeling, is excellent.

A variety of other XPCS and SAXS studies can be found in the literature. Among them are investigations of charge-stabilized $Sb_2O_5$ [41] and colloidal silica suspensions [42,43] revealing, e.g., evidence for a screening of hydrodynamic interactions [44]. Detailed studies were carried out on suspensions of colloidal polymer particles [45,46] and magnetic colloids (ferrofluids) [47].

### 5.3. Slow dynamics in polymer systems, membranes and liquids

The concepts of colloidal dynamics can in some cases be applied to polymer systems. This was shown in a study of spherical (polystyrene–polyisoprene) block copolymer

micelles dispersed in a (polystyrene) polymer matrix [5]. Similar to colloidal systems, one observes a slowing-down of the diffusivity on the lengthscale defined by the dominant interparticle correlations. Another application of the XPCS technique to polymer materials is the study of the equilibrium dynamics in an entangled polymer melt [48]. The time gap to the neutron spin-echo technique was recently bridged in a study of the dynamic behaviour of fluctuating smectic membranes [49–51], where correlation times down to 100 ns were measured.

Capillary wave dynamics on liquid surfaces has been investigated by XPCS in grazing incidence geometry [52]. Glycerol surfaces were illuminated under a grazing incident angle $\alpha_i$ well below the critical angle for total reflection thus limiting the penetration depth of the beam to the topmost 80 Å of the sample. The reflected beam had been recorded under an angle $\alpha_f \neq \alpha_i$ thus probing in-plane lengthscales $5\,\mu m < x_0 < 150\ \mu m$. High viscosity liquids, such as the prototypical glassformer glycerol, are expected to display (non-diffusive) overdamped capillary wave dynamics with a correlation rate

$$\Gamma(Q) = [\gamma(T)/2\eta(T)]Q, \tag{5.6}$$

where $\eta(T)$ is the dynamic viscosity and $\gamma(T)$ is the surface tension. This was in fact observed and Fig. 7 shows the measured correlation times $\tau_0 = 1/\Gamma(Q)$ as a function of $x_0 = 2\pi/Q$ for the different measured temperatures. The temperature dependence of the surface tension $\gamma(T)$ is known and the experiment data can thus provide information on the near surface viscosity of the liquid which happens to be in good agreement with published data for the bulk viscosity.

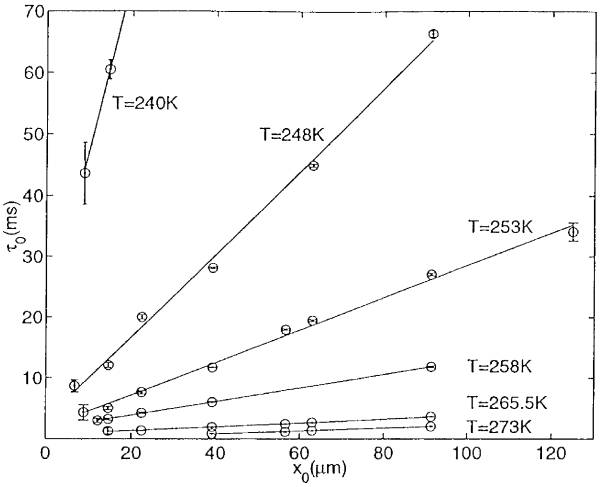


Fig. 7. Correlation times $\tau_0$ of overdamped capillary waves in glycerol for different temperatures as a function of the lateral lengthscale $x_0 = 2\pi/Q$ [52].

## 6. Slow dynamics in hard condensed matter systems

Coherent X-rays can probe disorder and dynamics in hard condensed matter systems on the same lengthscale range that is accessible to a conventional X-ray scattering experiment. Phenomena of interest involve the dynamics accompanying

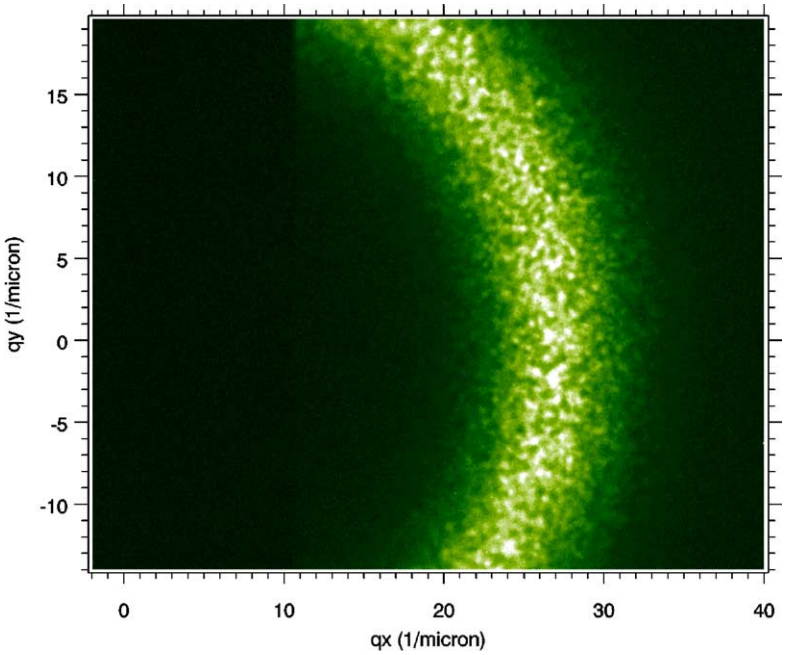


Fig. 8. Magnetic speckle pattern on the first order magnetic diffraction ring from meandering magnetic stripe domains in a 350-Å-thick film of $GdFe_2$ illuminated by a 15-μm diameter beam of circularly polarized X-rays tuned to the Gd $M_5$ resonance at 1183.6 eV [56].

domain formation in phase separating alloys or glasses, the dynamics of glass forming systems or the study of critical fluctuations [2].

Non-equilibrium fluctuations during domain coarsening were studied in a phase separating sodium borosilicate glass [53]. The sample with a critical composition for phase separation was allowed to equilibrate at high $T$ in the single phase state, then quenched to a lower temperature and allowed to separate isothermally into $B_2O_3$-rich and $SiO_2$-rich domains. These domains grow as a function of time. The theory of dynamic scaling predicts that the average structure factor does not change if the lengthscales are measured in units of the average domain size. This was in fact observed. Fluctuations about the average intensity were quantified by means of two-time correlation functions and it could be shown that the correlation times of fluctuations also obey a scaling law. Similar experiments were carried out in phase separating Al–Li alloys [54].

Coherent X-rays were also used to explore static disorder in magnetic systems. The (001) magnetic superlattice reflection of antiferromagnetic UAs was studied at 100 K with a coherent X-ray beam at the $M_{IV}$ absorption edge of uranium at 3.73 keV and shown to have a grainy speckle structure [55]. Magnetic speckles were also observed in resonant small angle scattering with soft X-rays from meandering magnetic stripe domains in a 350-Å-thick film of $GdFe_2$ [56]. The data were taken at the Gd $M_5$ absorption edge ($\lambda = 11$ Å) and Fig. 8 shows the recorded magnetic speckle pattern.

## 7. Conclusions and outlook

Scattering with coherent X-rays and X-ray photon correlation spectroscopy (XPCS) in particular have created considerable interest in the community of X-ray users although the technique is still in its nascent stage. Its impact will crucially depend on the development and use of fast two-dimensional detectors to exploit the regime of millisecond and microsecond dynamics at large $Q$. This will furthermore be crucial for the study of non-equilibrium phenomena and for the access to soft condensed matter materials that are often sensitive to radiation damage. Yet unexploited features of coherent beams are the polarization and polarization tunability and the possibility to tune the energy of the beam. One might finally anticipate new applications from fully coherent X-ray sources such as the planned X-ray free electron laser (FEL) sources.

## Acknowledgements

We wish to acknowledge the contributions of D.L. Abernathy, F. Bley, S. Brauer, C. Detlefs, S.B. Dierker, R. Fleming, E. Geissler, J. Goedkoop, J. Lal, J.F. Legrand, F. Livet, L. Lurio, A. Madsen, G. Meier, S.G.J. Mochrie, A. Moussaid, I. McNulty, A. Patkowski, R. Pindak, D. Riese, A. Robert, I.K. Robinson, A. Sandy, T. Seydel, S.K. Sinha, W. Steffen, G.B. Stephenson, M. Sutton, T. Thurn-Albrecht, M. Tolan, W. Vos, G. Wegdam, F. Yakhou and the help of the staff of the involved beamlines.

## References

[1] G. Grübel, J. Als-Nielsen, D. Abernathy, G. Vignaud, S. Brauer, G.B. Stephenson, S.G.J. Mochrie, M. Sutton, I.K. Robinson, R. Fleming, R. Pindak, S. Dierker, J.F. Legrand, ESRF Newslett. 20 (1994) 14; G. Grübel, D. Abernathy, G.B. Stephenson, S. Brauer, I. McNulty, S.G.J. Mochrie, B. McClain, A. Sandy, M. Sutton, E. Dufresne, I.K. Robinson, R. Fleming, R. Pindak, S. Dierker, ESRF Newslett. 23 (1995) 14.
[2] S. Brauer, G.B. Stephenson, M. Sutton, R. Brüning, E. Dufresne, S.G.J. Mochrie, G. Grübel, J. Als-Nielsen, D. Abernathy, Phys. Rev. Lett. 74 (1995) 2010.
[3] S.B. Dierker, R. Pindak, R.M. Fleming, I.K. Robinson, L. Berman, Phys. Rev. Lett. 75 (1995) 449.
[4] T. Thurn-Albrecht, W. Steffen, A. Patkowski, G. Meier, E.W. Fischer, G. Grübel, D. Abernathy, Phys. Rev. Lett. 77 (1996) 5437.
[5] S.G.J. Mochrie, A.M. Mayes, A.R. Sandy, M. Sutton, S. Brauer, G.B. Stephenson, D.L. Abernathy, G. Grübel, Phys. Rev. Lett. 78 (1997) 1275.
[6] See Refs. [17,20,22,23,25–29].
[7] P. Cloetens, R. Barrett, J. Baruchel, J.P. Guigay, M. Schlenker, J. Phys. D: Appl. Phys. 29 (1996) 133.
[8] A. Snigirev, I. Snigireva, V. Kohn, S. Kuznetsov, I. Schelokov, Rev. Sci. Instrum. 66 (1995) 5486;
C. Raven, A. Snigirev, I. Snigireva, P. Spanne, A. Souvorov, V. Kohn, Appl. Phys. Lett. 69 (1996) 1826.
[9] T. Gog, P.M. Len, G. Materlik, D. Bahr, C.S. Fadley, C. Sanchez-Hanke, Phys. Rev. Lett. 76 (1996) 3132.
[10] B.J. Berne, R. Pecora, Dynamic Light Scattering with Applications, John Wiley, New York 1976;
B. Chu, in: 2nd Edition Laser Light Scattering: Basic Principles and Practices, Academic Press, San Diego, 1991.
[11] M. Sutton, S.G.J. Mochrie, T. Greytak, S.E. Nagler, L.E. Berman, G.A. Held, G.B. Stephenson, Nature 353 (1991) 608.
[12] D. Attwood, K. Halbach, K.J. Kim, Science 228 (1985) 1265.
[13] M.V. Klein, T.E. Furtak, in: 2nd Edition, Optics, John Wiley, New York 1986.
[14] M. Born, E. Wolf, in: 6th Edition, Principles of Optics, Pergamon Press, Oxford 1985.
[15] G. Grübel, D.L. Abernathy, SPIEE 3154 (1997) 103.
[16] A.Q.R. Baron, A.I. Chumakov, H.F. Grunsteudel, H. Grunsteudel, L. Niesen, R. Rüffer, Phys. Rev. Lett. 77 (1996) 4808.
[17] D.L. Abernathy, G. Grübel, S. Brauer, I. McNulty, G.B. Stephenson, S.G.J. Mochrie, A.R. Sandy, N. Mulders, M. Sutton, J. Synchr. Rad. 5 (1998) 37.
[18] G. Grübel, J. Als-Nielsen, A.K. Freund, J. Phys. IV C9 (4) (1994) 27.
[19] A.R. Sandy, L.B. Lurio, S.G.J. Mochrie, A. Malik, G.B. Stephenson, SPIEE 3154 (1997) 27;
A.R. Sandy, L.B. Lurio, S.G.J. Mochrie, A. Malik, G.B. Stephenson, J.F. Pelletier, M. Sutton, J. Synchr. Rad. 6 (1999) 1174.
[20] O.K.C. Tsui, S.G.J. Mochrie, L.E. Berman, J. Synchr. Rad. 5 (1998) 30.
[21] I.K. Robinson, R. Pindak, R.M. Fleming, S.B. Dierker, K. Ploog, G. Grübel, D.L. Abernathy, J. Als-Nielsen, Phys. Rev. B 52 (1995) 9917;
D.L. Abernathy, J. Als-Nielsen, S.B. Dierker, R.M. Fleming, G. Grübel, R. Pindak, K. Ploog, I.K. Robinson, Solid-State Electron. 40 (1996) 531.

[22] Z.H. Cai, B. Lai, W.B. Yun, I. McNulty, K.G. Huang, T.P. Russel, Phys. Rev. Lett. 73 (1994) 82.
[23] J.L. Libbert, R. Pindak, S.B. Dierker, I.K. Robinson, Phys. Rev. B 56 (1997) 6454.
[24] F. Bley, F. Livet, J.C. Leroux, J.P. Simon, D. Abernathy, J. Als-Nielsen, G. Grübel, G. Vignaud, G. Dolino, J.F. Legrand, D. Camel, N. Menguy, M. Papoular, Acta Crystallogr. A 51 (1995) 746.
[25] I.A. Vartanyants, J. Pitney, J. Libbert, I.K. Robinson, Phys. Rev. B 55 (1997) 13193;
I.K. Robinson, J.L. Libbert, I.A. Vartanyants, J.A. Pitney, D.M. Smilgies, D.L. Abernathy, G. Grübel, Phys. Rev. B 60 (1999) 9965.
[26] I.K. Robinson, I.A. Vartanyants, G.J. Williams, M.A. Pfeifer, J.A. Pitney, Phys. Rev. Lett. 87 (2001) 195505.
[27] J. Miao, P. Charalambous, J. Kirz, D. Sayre, Nature 400 (1999) 342.
[28] J. Miao, K.O. Hodgson, D. Sayre, Proc. Natl. Acad. Sci. 98 (2001) 6641.
[29] R. Eisenhower, R. Gehrke, G. Materlik, M. Drakopolous, A. Simionovici, A. Snigirev, J. Synchr. Rad. 6 (1999) 1168.
[30] J.W. Goodman, in: J.C. Dainty (Ed.), Laser Speckle and Related Phenomena, Springer, Berlin, 1975;
J.W. Goodman, Statistical Optics, John Wiley, New York, 1985.
[31] S.K. Sinha, M. Tolan, A. Gibaud, Phys. Rev. B 57 (1998) 2740.
[32] P.N. Pusey, in: J.P. Hansen, D. Levesque, J. Zinn-Justin (Eds.), Liquids, Freezing and Glass Transition,, Les Houches, Session L1, Elsevier, Amsterdam 1989, p. 763.
[33] P.N. Segre, P.N. Pusey, Physica A 235 (1997) 9.
[34] F. Livet, F. Blay, J. Mainville, R. Caudron, S.G.J. Mochrie, E. Geissler, G. Dolino, D. Abernathy, G. Grübel, M. Sutton, Nucl. Instrum. Methods A 451 (2000) 596.
[35] D. Lumma, L.B. Lurio, S.G.J. Mochrie, M. Sutton, Rev. Sci. Instrum. 71 (2000) 3274.
[36] N.W. Ashcroft, J. Lekner, Phys. Rev. 145 (1966) 145.
[37] C.W.J. Beenakker, P. Mazur, Physica 120A (1983) 388;
C.W.J. Beenakker, P. Mazur, Physica 126A (1984) 349.
[38] R. Klein, B. d'Aguanno, in: W. Brown (Ed.), Light Scattering, Principles and Development, Clarendon Press, Oxford, 1996, p. 30.
[39] G. Grübel, A. Robert, D.L. Abernathy, Slow dynamics in complex systems, in: M. Tokuyama, I. Oppenheim (Eds.), Eighth Tohwa University International Symposium, 1999, p. 158.
[40] F. Zontone, A. Moussaid, A. Robert, G. Grübel, to be published.
[41] O.K.C. Tsui, S.G.J. Mochrie, Phys. Rev. E 57 (1998) 2030.
[42] G. Grübel, D.A. Abernathy, D.O. Riese, W.L. Vos, G.H. Wegdam, J. Appl. Crystallogr. 33 (2000) 424.
[43] D.O. Riese, W.L. Vos, G.H. Wegdam, F.J. Poelwijk, D.L. Abernathy, G. Grübel, Phys. Rev. E 61 (2000) 1676.
[44] D.O. Riese, G.H. Wegdam, W.L. Vos, R. Sprik, D. Feinstein, J.H.H. Bongaerts, G. Grübel, Phys. Rev. Lett. 85 (2000) 5460.
[45] D. Lumma, L.B. Lurio, M.A. Borthwick, P. Falus, S.G.J. Mochrie, Phys. Rev. E 62 (2000) 8258.
[46] L.B. Lurio, D. Lumma, A.R. Sandy, M.A. Borthwick, P. Falus, S.G.J. Mochrie, J.F. Pelletier, M. Sutton, L. Regan, A. Malik, G.B. Stephenson, Phys. Rev. Lett. 84 (2000) 785.
[47] J. Lal, D. Abernathy, L. Auvray, O. Diat, G. Grübel, Eur. Phys. J. E 4 (2001) 263.
[48] D. Lumma, M.A. Borthwick, P. Falus, L.B. Lurio, S.G.J. Mochrie, Phys. Rev. Lett. 86 (2001) 2042.
[49] A.C. Price, L.B. Sorensen, S.D. Kevan, J. Toner, A. Poniewierski, R. Kolyst, Phys. Rev. Lett. 82 (1999) 755.
[50] A. Fera, I.P. Dolbyna, G. Grübel, H.G. Muller, B.I. Ostrovskii, A.N. Shalaginov, W.H. deJeu, Phys. Rev. Lett. 85 (2000) 2316.
[51] I. Sikharulidze, I.P. Dolbyna, A. Fera, A. Madsen, B.I. Ostrovskii, W. de Jeu, Phys. Rev. Lett. 88 (2002) 115503.
[52] T. Seydel, A. Madsen, M. Tolan, G. Grübel, W. Press, Phys. Rev. B 63 (2001) 73409.
[53] A. Malik, A.R. Sandy, L.B. Lurio, G.B. Stephenson, S.G.J. Mochrie, I. McNulty, M. Sutton, Phys. Rev. Lett. 81 (1998) 5832.
[54] J. Mainville, F. Bley, F. Livet, E. Geissler, J.F. Legrand, D. Abernathy, G. Grübel, S.G.J. Mochrie, M. Sutton, J. Appl. Crystallogr. 30 (1997) 828;
F. Livet, F. Bley, E. Geissler, R. Goudron, M. Sutton, G. Grübel, Phys. Rev. E 63 (2001) 36108.
[55] F. Yakhou, A. Letoublon, F. Livet, M. de Boissieu, F. Bley, C. Vettier, ESRF Newslett. 32 (1999) 12.
[56] J.F. Peters, M.A. de Fries, J. Miguel, O. Toulemonde, J. Goedkoop, ESRF Newslett. 34 (2000) 15.